Crossover from electromagnetically induced transparency to Autler-Townes splitting in open V-type molecular systems

Chengjie Zhu, Chaohua Tan, and Guoxiang Huang[*]

State Key Laboratory of Precision Spectroscopy and Department of Physics, East China Normal University, Shanghai 200062, China

We investigate electromagnetically induced transparency (EIT) and Autler-Townes splitting (ATS) in an open V-type molecular system. Through detailed analytical calculations of the absorption spectrum of a probe laser field using the residue theorem and spectrum decomposition, we find that EIT may occur and a crossover from EIT to ATS exists for hot molecules. However, there is no EIT and hence no EIT-ATS crossover for cold molecules. Furthermore, we prove that for hot molecules EIT is allowed even for a counter-propagating configuration. We provide explicit formulas of EIT conditions and widths of EIT transparency windows of the probe field when hot molecules work in copropagating and counter-propagating configurations, respectively. Our theoretical result agrees well with the recent experimental ones reported by Lazoudis *et al.* [Phys. Rev. A **83**, 063419 (2011)].

PACS number(s): 42.50.Gy, 42.50.Hz, 33.40.+f

I. INTRODUCTION

Quantum coherent phenomena occur widely in multilevel systems interacting resonantly with electromagnetic fields. ln 1955, Autler and Townes [1] showed that an absorption line of molecular transition can split into two Lorentzian lines (a doublet) when one of two levels involved in the transition is coupled to a third one by a strong microwave field. Such a doublet is now called Autler-Townes splitting (ATS). In 1961, Fano [2] showed that two resonant modes decaying via a common reservoir may yield a quantum destructive interference between the modes mediated by the reservoir. This phenomenon is now called Fano interference.

In recent years, much attention has been paid to the study of electromagnetically induced transparency (EIT). By use of the quantum interference effect induced by a control field, significant suppression of absorption of a probe field can be realized, together with a large reduction in group velocity and giant enhancement of Kerr nonlinearity [3]. Due to EIT, a transparency window appears in the probe-field absorption spectrum, which can generally be decomposed into two Lorentzian terms, together with one (or several) Fano interference term(s). Thus the EIT line shape displays characters of both ATS and Fano interference.

In the past two decades, EIT and related quantum interference effects in various atomic systems have been studied intensively in both theory and experiment, and a large amount of research progress has been achieved [3,4]. Similar phenomena in molecular systems have also been explored in recent years. Especially, EIT has been observed in ^{7}Li$_2$ [5,6], K$_2$ [7], and Na$_2$ vapors [8,9], in acetylene molecules filled in hollow-core photonic crystal fibers [10,11] and in photonic microcells [12], and in Cs$_2$ in a vapor cell [13].

Although many experiments have been carried out, up to now the theoretical approach to EIT in molecular systems is less developed. Unlike atoms, even the simplest molecules are open systems in which each excited molecular rovibrational level is radiatively coupled to many other energy levels. Furthermore, all related experiments were made by using thermal molecular vapors, which involve Doppler broadening and other decoherence effects. Therefore, EIT in molecular systems is more challenging not only for experimental observation, but also for theoretical analysis. Because of the difficulty of the analytical approach, numerical simulations are usually done. However, the result of numerical simulations generally does not easily clarify various EIT characters, and distinguishing ATS from EIT clearly is also hard.

In the present work, we develop an analytical approach to EIT and ATS in an open V-type molecular system. Through detailed analytical calculations on the absorption spectrum of a probe field using the residue theorem and spectrum-decomposition method, we find that EIT is possible and a crossover from EIT to ATS exists for hot molecules with Doppler broadening. In contrast, there is no EIT and hence no EIT-ATS crossover for cold molecules. We also find that for hot molecules EIT is allowed even for a counter-propagating configuration of the probe and control fields. We provide explicit formulas for EIT conditions, widths of EIT transparency windows, and group velocities of the probe field when hot molecules work in copropagating and counter-propagating configurations, respectively. Our theoretical result agrees well with the recent experiment reported by Lazoudis *et al.* [9].

Before proceeding, we note that the spectrum-decomposition method was first proposed by Agarwal [14] for analyzing probe-field absorption in several typical three-level atomic systems, which can isolate the precise nature of quantum interference induced by a control field. However, Agarwal's method is valid only for a strong control field. Recently, Anisimov and Kocharovskaya [15] considered the absorption line shape of a Λ-type system in view of resonant poles and successfully explained the nature of quantum destructive interference for a weak control field. Recently, Abi-Salloum [16] distinguished EIT and ATS for similar atomic systems discussed in Ref. [14] using the method in Ref. [15], but with this method one cannot obtain the quantum interference term for a strong control field analytically. In a recent work, Anisimov *et al.* suggested a computational fitting technique to objectively discern ATS versus EIT [17] from experimental data. Very recently, an experimental investigation of the crossover between ATS and EIT was carried out by Giner *et al.* [18] using the method proposed by Anisimov

*gxhuang@phys.ecnu.edu.cn

et al. [17]. These works are significant, especially for clarifying the difference between EIT and ATS and some related concepts of quantum interference.

From the works [14–17] mentioned above, we can define EIT as a quantum coherent phenomenon, where not only is a transparency window opened in the probe-field absorption spectrum, but also a quantum *destructive* interference induced by the control field should appear. Note that this definition of EIT is very general, and the reason for quantum destructive interference is not specified. Quantum destructive interference can be induced by different physical mechanisms in different systems, including the V-type system we consider below.

The present work is related to Refs. [14–17] and, in particular, to the experimental work in Ref. [9]. However, systems considered in Refs. [14] are only for cold atomic systems. It has been shown by the authors of Refs. [14–17] that an EIT is impossible for a cold V-type system because the quantum interference in such a system is constructive. Our work is an analytical approach to discern ATS and EIT in Doppler-broadened molecular systems. We explicitly show that a quantum destructive interference and hence EIT may occur in V-type molecular systems. Furthermore, our analytical approach developed below is valid for an arbitrary control field and can demonstrate clearly the contribution of Doppler broadening and various quantum interference characters (EIT, ATS, and EIT-ATS crossover) in a clear way.

The article is organized as follows. Section II presents our theoretical model for the open V-type molecular system. Section III provides the solution of the Maxwell-Bloch equation and discusses the absorption and dispersion properties of probe field. The spectrum decomposition and EIT-ATS crossover is analyzed in detail and a comparison between our theoretical result with the experimental one by Lazoudis *et al.* [9] is given. Section IV studies the linear absorption of the probe field in corresponding cold molecular system. Section V discusses the roles of saturation and hole burning in the V-type system. Finally, Section VI summarizes the main results obtained in our work.

II. MODEL AND GENERAL SOLUTION

A. The Model

Our model is the same as that used in Ref. [9]. An open, three-level, V-type Na_2 molecular system [Fig. 1(a)] consists of two excited upper molecular states, $A^1\Sigma_u^+(v'=6, J'=13)$ (labeled $|2\rangle$) and $A^1\Sigma_u^+(v'=7, J'=13)$ (labeled $|3\rangle$), and a ground state $X^1\Sigma_g^+(v''=0, J''=14)$ (labeled $|1\rangle$). A probe (control) field with center frequency ω_p (ω_c) and center wave vector $\mathbf{k}_p$ ($\mathbf{k}_c$) couples to the excited state $|3\rangle$ ($|2\rangle$) and the ground state $|1\rangle$. The electric field acting on the molecule system is of the form $\mathbf{E} = \sum_{l=p,c} \mathbf{e}_l \mathcal{E}_l(z,t)e^{i(\mathbf{k}_l \cdot \mathbf{r} - \omega_l t)} + \text{c.c.}$, where $\mathbf{e}_l$ ($\mathcal{E}_l$) is the unit polarization vector (envelope) of the lth electric-field component. Both upper exited states ($|2\rangle$ and $|3\rangle$) are considered to decay spontaneously to ground state $|1\rangle$ at decay rates of Γ_{12} and Γ_{13}, respectively. However, due to the open character of the system, the molecule occupying the excited states $|2\rangle$ and $|3\rangle$ may follow various relaxation pathways and decay to many ground states besides state $|1\rangle$. For simplicity, all these states are represented by state $|4\rangle$. The decay rate Γ_{4l} ($l=2,3$) indicates the spontaneous emission
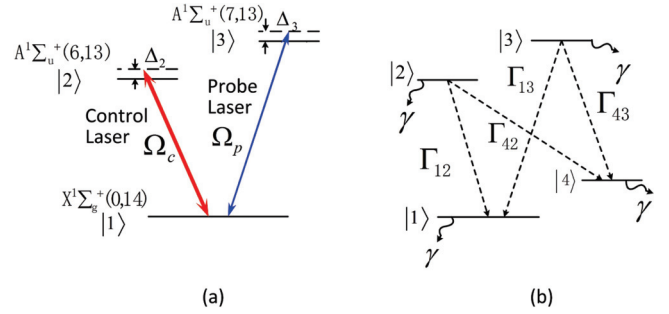

FIG. 1. (Color online) (a) V-type three-level scheme of the Na_2 molecular system. The ground state $X^1\Sigma_g^+(v''=0, J''=14)$ (labeled $|1\rangle$) is coupled to the excited state $A^1\Sigma_u^+(v'=6, J'=13)$ (labeled $|2\rangle$) by the control laser field with half Rabi frequency Ω_c and, also, to the excited state $A^1\Sigma_u^+(v'=7, J'=13)$ (labeled $|3\rangle$) by the probe laser field with half Rabi frequency Ω_p. Δ_2 and Δ_3 are detunings of the control and probe fields, respectively. (b) The molecule occupying excited states $|2\rangle$ and $|3\rangle$ follow various relaxation pathways and decay to many ground-state levels besides state $|1\rangle$. All these states are represented by state $|4\rangle$. Γ_{jl} denotes the spontaneous decay from state $|l\rangle$ to state $|j\rangle$. γ is the rate at which σ_{jl} relaxes to its equilibrium value σ_{jl}^{eq}.

rate of level $|l\rangle$ to level $|4\rangle$ [see Fig. 1(b)]. The decay rate γ is the rate at which σ_{jl} relaxes to its thermodynamical equilibrium value σ_{jl}^{eq}.

For hot molecules, Doppler broadening must be taken into account because the experiments are carried out in a heat-pipe oven [9]. Under electric-dipole and rotating-wave approximations, the interaction Hamiltonian of the system in the interaction picture reads

$$
\hat{H} = -\hbar(\Omega_c e^{i[\mathbf{k}_c \cdot (\mathbf{r}+\mathbf{v}t)-\omega_c t]}|2\rangle\langle 1| \\
+ \Omega_p e^{i[\mathbf{k}_p \cdot (\mathbf{r}+\mathbf{v}t)-\omega_p t]}|3\rangle\langle 1| + \text{c.c.}), \tag{1}
$$

where $\mathbf{v}$ is the molecular velocity and $\Omega_{c(p)} = (\mathbf{e}_{c(p)} \cdot \boldsymbol{\mu}_{21(31)})\mathcal{E}_{c(p)}/(2\hbar)$ is the half Rabi frequency of the probe (control) field, with $\boldsymbol{\mu}_{jl}$ the electric-dipole matrix element associated with the transition from state $|j\rangle$ to state $|l\rangle$. Density matrix elements in the interaction picture are $\sigma_{jl} = \rho_{jl}\exp(i\{(\mathbf{k}_l - \mathbf{k}_j) \cdot (\mathbf{r}+\mathbf{v}t) - [(E_l - E_j)/\hbar - \Delta_l + \Delta_j]t\})$ ($j,l=1$–4); here $\Delta_1 = 0$, $\Delta_2 = \omega_c - (E_2 - E_1)/\hbar$, and $\Delta_3 = \omega_p - (E_3 - E_1)/\hbar$ are detunings and ρ_{jl} are the density matrix elements in the Schrödinger picture, with E_j being the eigenenergy of level $|j\rangle$. The Bloch equation governing the evolution of σ_{jl} reads

$$
i\frac{\partial}{\partial t}\sigma_{11} + i\gamma(\sigma_{11} - \sigma_{11}^{\text{eq}}) - i\Gamma_{12}\sigma_{22} \\
- i\Gamma_{13}\sigma_{33} + \Omega_c^*\sigma_{21} - \Omega_c\sigma_{21}^* + \Omega_p^*\sigma_{31} - \Omega_p\sigma_{31}^* = 0, \tag{2a}
$$

$$
i\frac{\partial}{\partial t}\sigma_{22} + i\gamma(\sigma_{22} - \sigma_{22}^{\text{eq}}) + i\Gamma_2\sigma_{22} + \Omega_c\sigma_{21}^* - \Omega_c^*\sigma_{21} = 0, \tag{2b}
$$

$$
i\frac{\partial}{\partial t}\sigma_{33} + i\gamma(\sigma_{33} - \sigma_{33}^{\text{eq}}) + i\Gamma_3\sigma_{33} + \Omega_p\sigma_{31}^* - \Omega_p^*\sigma_{31} = 0, \tag{2c}
$$

$$
i\frac{\partial}{\partial t}\sigma_{44} + i\gamma(\sigma_{44} - \sigma_{44}^{\text{eq}}) - i\Gamma_{42}\sigma_{22} - i\Gamma_{43}\sigma_{33} = 0, \tag{2d}
$$

$$i\frac{\partial}{\partial t}\sigma_{21} + d_{21}\sigma_{21} + \Omega_c(\sigma_{11} - \sigma_{22}) - \Omega_p\sigma_{32}^* = 0, \tag{2e}$$

$$i\frac{\partial}{\partial t}\sigma_{31} + d_{31}\sigma_{31} + \Omega_p(\sigma_{11} - \sigma_{33}) - \Omega_c\sigma_{32} = 0, \tag{2f}$$

$$i\frac{\partial}{\partial t}\sigma_{32} + d_{32}\sigma_{32} + \Omega_p\sigma_{21}^* - \Omega_c^*\sigma_{31} = 0, \tag{2g}$$

where $d_{21} = -\mathbf{k}_c \cdot \mathbf{v} + \Delta_2 - \Delta_1 + i\gamma_{21}$, $d_{31} = -\mathbf{k}_p \cdot \mathbf{v} + \Delta_3 - \Delta_1 + i\gamma_{31}$, and $d_{32} = -(\mathbf{k}_p - \mathbf{k}_c) \cdot \mathbf{v} + \Delta_3 - \Delta_2 + i\gamma_{32}$, with $\gamma_{jl} = (\Gamma_j + \Gamma_l)/2 + \gamma + \gamma_{jl}^{col}$ (j,l = 1-3). $\Gamma_l = \sum_{j\neq l}\Gamma_{jl}$, with Γ_{jl} denoting the rate per molecule at which the population decays from state $|l\rangle$ to state $|j\rangle$. The quantity γ_{jl}^{col} is the dephasing rate due to processes such as elastic collisions. σ_{jj}^{eq} is the thermal equilibrium value of σ_{jj} when all electric fields are absent. Equation (2) satisfies $\sum_{j=1}^4 \sigma_{jj} = 1$, with $\sum_{j=1}^4 \sigma_{jj}^{eq} = 1$. At thermal equilibrium, the population in the excited states is much smaller than that in the ground state, i.e., $\sigma_{22}^{eq} = \sigma_{33}^{eq} \simeq 0$ and hence $\sigma_{11}^{eq} + \sigma_{44}^{eq} = 1$.

Evolution of the electric field is governed by the Maxwell equation $\nabla^2\mathbf{E} - (1/c^2)\partial^2\mathbf{E}/\partial t^2 = [1/(\epsilon_0 c^2)]\partial^2\mathbf{P}/\partial t^2$, with the electric polarization intensity given by

$$\mathbf{P} = \mathcal{N}_a \int_{-\infty}^{+\infty} dv f(v)[\boldsymbol{\mu}_{13}\sigma_{31}e^{i(k_p \cdot z - \omega_p t)}$$
$$+ \boldsymbol{\mu}_{12}\sigma_{21}e^{i(k_c \cdot z - \omega_c t)} + \text{c.c.}], \tag{3}$$

where $\mathcal{N}_a$ is the molecular density and $f(v)$ is the molecular velocity distribution function. For simplicity, we have assumed that electric-field wave vectors are along the z direction, i.e., $\mathbf{k}_{p,c} = (0,0,k_{p,c})$. Under the slowly-varying envelope approximation, the Maxwell equation reduces to

$$i\left(\frac{\partial}{\partial z} + \frac{1}{c}\frac{\partial}{\partial t}\right)\Omega_p + \kappa_{13}\int_{-\infty}^{+\infty} dv f(v)\sigma_{31} = 0, \tag{4}$$

where $\kappa_{13} = \mathcal{N}_a\omega_p|\boldsymbol{\mu}_{31}|^2/(2\hbar\epsilon_0 c)$, with c the light speed in vacuum.

B. General solution

The base state of the system, i.e., the time-independent solution of the Maxwell-Bloch equations (2) and (4), in the absence of the probe field is

$$\sigma_{11}^{(0)} = \gamma(\gamma + \Gamma_3)\left(\gamma + \Gamma_2 + 2\gamma_{21}\frac{|\Omega_c|^2}{|d_{21}|^2}\right)\frac{\sigma_{11}^{eq}}{D_0}, \tag{5a}$$

$$\sigma_{22}^{(0)} = 2\gamma\gamma_{21}(\gamma + \Gamma_3)\frac{|\Omega_c|^2}{|d_{21}|^2}\frac{\sigma_{11}^{eq}}{D_0}, \tag{5b}$$

$$\sigma_{21}^{(0)} = \frac{\Omega_c}{d_{21}}\left(\sigma_{22}^{(0)} - \sigma_{11}^{(0)}\right) = -\frac{\Omega_c}{d_{21}}\gamma(\gamma + \Gamma_2)(\gamma + \Gamma_3)\frac{\sigma_{11}^{eq}}{D_0}, \tag{5c}$$

and $\sigma_{33}^{(0)} = \sigma_{31}^{(0)} = \sigma_{32}^{(0)} = 0$, where $D_0 = 2\gamma_{21}(|\Omega_c|^2/|d_{21}|^2)(\gamma + \Gamma_{42})(\gamma + \Gamma_3) + \gamma(\gamma + \Gamma_3)[\gamma + \Gamma_2 + 2\gamma_{21}(|\Omega_c|^2/|d_{21}|^2)]$. Note that in the above expressions $d_{21} = d_{21}(v) = -k_c v + \Delta_2 - \Delta_1 + i\gamma_{21}$, $d_{31} = d_{31}(v) = -k_p v + \Delta_3 - \Delta_1 + i\gamma_{31}$, and $d_{32} = d_{32}(v) = -(k_p - k_c)v + \Delta_3 - \Delta_2 + i\gamma_{32}$. Also, note that $\sigma_{44}^{(0)} = 1$ and all other $\sigma_{ij}^{(0)} = 0$

if $\gamma = 0$. However, in our thermal molecular system $\gamma \neq 0$ ($\gamma \approx 3$ MHz in the experiment [9]), thus $\sigma_{ll}^{(0)}$ ($l = 1,2$) and $\sigma_{21}^{(0)}$ take nonzero values. In particular, for large Ω_c molecules populate mainly in $|1\rangle$ and $|2\rangle$, i.e., the population in $|4\rangle$ is small (about 10% of the total number of molecules).

At first order in Ω_p, the populations and the coherence between state $|1\rangle$ and state $|2\rangle$ are not changed. It is easy to get the solution

$$\Omega_p^{(1)} = Fe^{i[K(\omega)z - \omega t]}, \tag{6}$$

$$\sigma_{31}^{(1)} = \frac{d_{21}^*(\omega + d_{32})\sigma_{11}^{(0)} - |\Omega_c|^2(\sigma_{11}^{(0)} - \sigma_{22}^{(0)})}{d_{21}^* D}Fe^{i[K(\omega)z - \omega t]}, \tag{7}$$

$$\sigma_{32}^{(1)} = \frac{-(\omega + d_{31})\Omega_c^*(\sigma_{11}^{(0)} - \sigma_{22}^{(0)}) + d_{21}^*\Omega_c^*\sigma_{11}^{(0)}}{d_{21}^* D}Fe^{i[K(\omega)z - \omega t]}, \tag{8}$$

where $D = |\Omega_c|^2 - (\omega + d_{31})(\omega + d_{32})$ and F is a constant. The dispersion relation $K(\omega)$ [21] reads

$$K(\omega) = \frac{\omega}{c} + \kappa_{13}\int_{\infty}^{\infty} dv f(v)$$
$$\times \frac{d_{21}^*(\omega + d_{32})\sigma_{11}^{(0)} - |\Omega_c|^2(\sigma_{11}^{(0)} - \sigma_{22}^{(0)})}{d_{21}^*[|\Omega_c|^2 - (\omega + d_{31})(\omega + d_{32})]}. \tag{9}$$

Note that the integrand in the dispersion relation, (9), depends on three factors. The first is the ac Stark effect induced by the control field, reflected in the denominator, corresponding to the appearance of dressed states out of states $|1\rangle$ and $|2\rangle$, by which two Lorentzian peaks in the probe-field absorption spectrum are shifted from their original positions. The second, reflected in the numerator, is proportional to $\sigma_{11}^{(0)} - \sigma_{22}^{(0)}$. The appearance of nonzero $\sigma_{22}^{(0)}$ is due to the saturation effect induced by the control field. When the control field grows, the saturation effect increases. When $|\Omega_c|^2/|d_{21}|^2 \gg 1$, $\sigma_{22}^{(0)} \approx \sigma_{11}^{(0)}$, and hence the second term in the numerator will disappear. The third is the Doppler effect, reflected by $d_{jl} = d_{jl}(v)$ and the molecular velocity distribution $f(v)$, which may increase or decrease probe-field absorption, as shown below.

III. HOT MOLECULES

For a thermal gas, the integration in Eq. (9) over the molecular velocity v must be carried out properly. In thermal equilibrium, the velocity distribution function is Maxwellian $f(v) = [1/(\sqrt{\pi}\,v_T)]\exp(-v^2/v_T^2)$, where $v_T = \sqrt{2k_B T/M}$ is the most probable speed, and M is the molecular mass. The integration in Eq. (9) with the Maxwellian distribution leads to a particular combination of error functions, which is very inconvenient for a systematic analytical approach. As done in Refs. [19,20], we adopt the Lorentzian velocity distribution profile $f(v) = v_T/[\sqrt{\pi}(v_T^2 + v^2)]$ to replace the Maxwellian distribution.

We are interested in two cases: copropagating (i.e., $k_p \approx k_c$) and counter-propagating (i.e., $k_p \approx -k_c$), which are discussed separately.
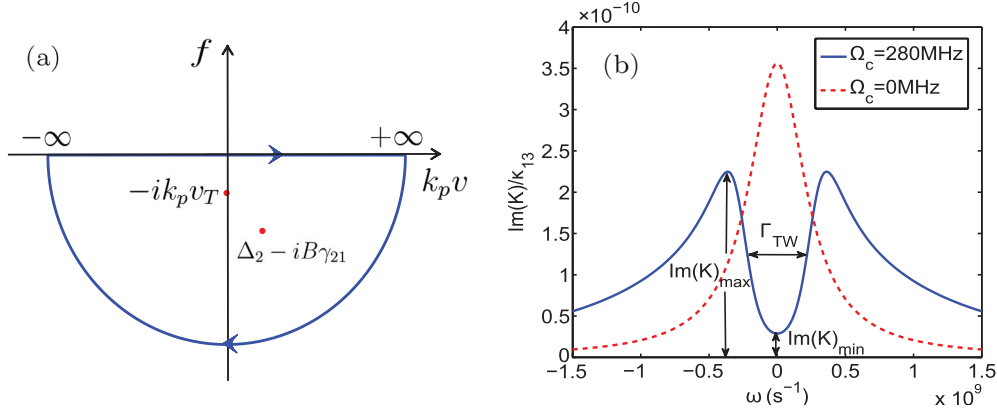
FIG. 2. (Color online) (a) Two poles, $(\Delta_2, -iB\gamma_{21})$ and $(0, -ik_p v_T)$ (represented by filled circles), in the lower half complex plane of the integrand in Eq. (9). The closed curve with arrows is the contour chosen for calculating the integration in Eq. (9) using residue theorem. (b) Probe-field absorption spectrum Im(K) as a function of ω. The solid (dashed) line represent $|\Omega_c| = 280$ MHz ($|\Omega_c| = 0$ MHz). Definitions of Im(K)$_{\min}$ and Im(K)$_{\max}$ and the width of the transparency window $\Gamma_{\rm TW}$ are indicated.

A. Copropagating configuration

In this case, one has $d_{21} = -k_p v + \Delta_2 + i\gamma_{21}$, $d_{31} = -k_p v + \Delta_3 + i\gamma_{31}$, and $d_{32} = \Delta_3 - \Delta_2 + i\gamma_{32}$. The second term on the right-hand side of Eq. (9) can be calculated by considering a contour integration [see Fig. 2(a)] in a complex plane of $k_p v$ and using the residue theorem [22,23].

We find two poles in the lower half complex plane for the integrand of Eq. (9),

$$k_p v = \Delta_2 - iB\gamma_{21}, \quad k_p v = -ik_p v_T, \qquad (10)$$

with $B = \{1 + [2|\Omega_c|^2/\gamma_{21}(\gamma + \Gamma_2)][1 + (\gamma + \Gamma_{42})/\gamma]\}^{1/2}$. By taking a contour consisting of a real axis and a semicircle in the lower half complex plane [see the curves with arrows shown in Fig. 2(a)], we can calculate the integration in Eq. (9) analytically by just calculating the residues corresponding to the two poles and obtain the exact and explicit result for the integration. Since the general expression is lengthy, here we just write down the one with $\Delta_2 = \Delta_3 = 0$ and the condition $\Delta\omega_D \gg \gamma_{jl}, \gamma$:

$$K(\omega) = \omega/c + \mathcal{K}_1 + \mathcal{K}_2, \tag{11a}$$

$$\mathcal{K}_1 = \kappa'_{13} \frac{(\omega + i\gamma_{32})[\Gamma_3(1 - B^2)\gamma_{31} + 2|\Omega_c|^2] - i\Gamma_3|\Omega_c|^2(1 + B)}{\gamma \Gamma_3 B (\Delta\omega_D^2 - B^2\gamma_{31}^2)[|\Omega_c|^2 - (\omega + i\gamma_{31} + iB\gamma_{31})(\omega + i\gamma_{32})]}, \tag{11b}$$

$$\mathcal{K}_2 = \kappa'_{13} \frac{(\omega + i\gamma_{32})[\Gamma_3(\gamma_{31}^2 - \Delta\omega_D^2) + 2\gamma_{31}|\Omega_c|^2] - i\Gamma_3|\Omega_c|^2(\gamma_{31} + \Delta\omega_D)}{[\gamma \Gamma_3(\gamma_{31}^2 - \Delta\omega_D^2) + 2\gamma_{31}|\Omega_c|^2\Gamma_{13}][|\Omega_c|^2 - (\omega + i\gamma_{31} + i\Delta\omega_D)(\omega + i\gamma_{32})]}, \tag{11c}$$

where $\kappa'_{13} = \sqrt{\pi}\kappa_{13}\gamma\sigma_{11}^{\rm eq}$ and $\Delta\omega_D = k_p v_T$ (Doppler width). Note that for cold molecules the second pole in Eq. (10) is absent, thus $\mathcal{K}_2 = 0$. However, for hot molecules, due to the Doppler effect one has $\mathcal{K}_2 \neq 0$, and hence the system may display very different quantum interference characters that do not exist for cold molecules.

In most cases, $K(\omega)$ can be Taylor expanded around the center frequency (corresponding to $\omega = 0$) of the probe field, i.e., $K(\omega) = K_0 + K_1\omega + \cdots$, where $K_j \equiv (\partial^j K/\partial\omega^j)_{\omega=0}$. Here Re($K_0$) and Im($K_0$) describe, respectively, the phase shift and absorption per unit length, and Re($1/K_1$) ($\equiv v_g$) gives the group velocity of the probe field.

1. Transparency window in the absorption spectrum

Shown in Fig. 2(b) is the probe-field absorption spectrum Im(K) as a function of ω. The solid (dashed) line is for

$|\Omega_c| = 280$ MHz ($|\Omega_c| = 0$), with other parameters given by $\Gamma_{j2} \approx \Gamma_{j3}$ ($j = 1, 4$) = 4.08×10^7 Hz, $\gamma_{32}^{\rm col} \approx \gamma_{21}^{\rm col} \approx \gamma_{31}^{\rm col} = 5 \times 10^6$ Hz, $\gamma = 3 \times 10^6$ Hz, and $\Delta\omega_D = 0.6$ GHz. One sees that the absorption spectrum for $|\Omega_c| = 0$ has only a single peak (the dashed line). However, a significant transparency window is opened for a nonzero Ω_c (the solid line). The minimum [Im(K)$_{\min}$], maximum [Im(K)$_{\max}$], and width of the transparency window ($\Gamma_{\rm TW}$) are defined in Fig. 2(b).

From Eq. (11), we get

$$\text{Im}(K)_{\min} \approx \frac{\kappa'_{13}}{\Delta\omega_D} \frac{x + z/2 + z\sqrt{x}/2}{(1 + \sqrt{x})(x + z/2)(1 + 2\sqrt{x}/z)}, \tag{12}$$

where $x \equiv |\Omega_c|^2\gamma_{31}/(\gamma_{32}\Delta\omega_D^2)$ and $z \equiv \gamma_{31}/(\Delta\omega_D)$ are two dimensionless parameters. At the temperature in the experiment carried out in Ref. [9], one has $z \ll 1$ because $\gamma_{31} \ll \Delta\omega_D$. From Eq. (12) we obtain the following conclusions:

(1) For a large $|\Omega_c|$, i.e., $|\Omega_c| \gg \sqrt{\gamma_{32}/\gamma_{31}}\Delta\omega_D$ (and hence $x \gg 1$), $\text{Im}(K)_{\min}$ is vanishing small.

(2) For a small $|\Omega_c|$, i.e., $|\Omega_c| \ll \sqrt{\gamma_{32}/\gamma_{31}}\Delta\omega_D$ but with $|\Omega_c| \approx \sqrt{\gamma_{31}\gamma_{32}}$ (and hence $x \ll 1$, $\sqrt{x}/z \sim 1$), $\text{Im}(K)_{\min}$ is small.

The first conclusion is obvious because the reduction in $\text{Im}(K)_{\min}$ for larger $|\Omega_c|$ is due to the ATS effect. The maximum of $\text{Im}(K)$ is found to be $\text{Im}(K)_{\max} \approx \kappa'_{13}/\Delta\omega_D$, located at $\omega \approx \pm\Omega_c$. Using these results we obtain the expression for the width of the transparency window:

$$\Gamma_{\text{TW}} \approx 2\left(\frac{2|\Omega_c|^2 + \Delta\omega_D^2 - \Delta\omega_D\sqrt{\Delta\omega_D^2 + 4|\Omega_c|^2}}{2}\right)^{1/2}.$$

(13)

However, the second conclusion is not easy to understand because, from the conventional viewpoint, for a small $|\Omega_c|$ the Doppler broadening suppresses the quantum interference effect induced by Ω_c. In the following, we show that this conclusion is not correct for the V-type system with the Doppler effect. In fact, the suppression of $\text{Im}(K)_{\min}$ for small $|\Omega_c|$ can be obtained because the Doppler effect can contribute a quantum *destructive* interference to the system.

2. EIT-ATS crossover

Now we extend the spectrum-decomposition method introduced in Refs. [14–17] to analyze the detailed characters of the probe-field absorption explicitly. $\mathcal{K}_j$ $(j = 1,2)$ in Eq. (11) can be easily decomposed as

$$\mathcal{K}_j = \alpha_j\left(\frac{A_{j+}}{\omega - \delta_{j+}} + \frac{A_{j-}}{\omega - \delta_{j-}}\right),$$

(14)

where α_j and $A_{j\pm}$ are constants, and δ_{j+} and δ_{j-} are two spectrum poles of $\mathcal{K}_j$; all of these are given explicitly in the Appendix.

Our aim is to analyze the quantum interference effect, for which the expression of $\text{Im}(\mathcal{K}_j)$ is required. However, their general expressions are long and complicated. In order to illustrate the quantum interference effect in a clear way, we decompose $\text{Im}(\mathcal{K}_j)$ according to different regions of Ω_c as follows.

(i) *Weak control-field region* (i.e., $\Omega_c < \Omega_{\text{ref}} \equiv \Delta\omega_D/2$): Using a similar approach by Anisimov *et al.* [15,17], we obtain the imaginary part of $\mathcal{K}_j$ in this region as

$$\text{Im}(\mathcal{K}_j) = \alpha_j\left(\frac{C_{j+}}{\omega^2 + W_{j+}^2} + \frac{C_{j-}}{\omega^2 + W_{j-}^2}\right),$$

(15)

with real constants

$$C_{j+} = W_{j+}\left(W_{j+} - \Gamma_j^w\right)/(W_{j+} - W_{j-}), \quad \text{(16a)}$$

$$C_{j-} = -W_{j-}\left(W_{j-} - \Gamma_j^w\right)/(W_{j+} - W_{j-}), \quad \text{(16b)}$$

$$W_{1\pm} = \tfrac{1}{2}[\gamma_{31}(1+B) + \gamma_{32}$$
$$\pm\sqrt{[\gamma_{31}(1+B) - \gamma_{32}]^2 - 4|\Omega_c|^2}], \quad \text{(16c)}$$

$$W_{2\pm} = \tfrac{1}{2}[\gamma_{31} + \Delta\omega_D + \gamma_{32}$$
$$\pm\sqrt{(\gamma_{31} + \Delta\omega_D - \gamma_{32})^2 - 4|\Omega_c|^2}], \quad \text{(16d)}$$

where $\Gamma_1^w = \gamma_{32} - \Gamma_3|\Omega_c|^2(1+B)/[\Gamma_3(1-B^2)\gamma_{31} + 2|\Omega_c|^2]$ and $\Gamma_2^w = \gamma_{32} - \Gamma_3|\Omega_c|^2(\gamma_{31} + \Delta\omega_D)/[\Gamma_3(\gamma_{31}^2 - \Delta\omega_D^2) + 2\gamma_{31}|\Omega_c|^2]$.

Shown in Fig. 3(a) are results for $\text{Im}(\mathcal{K}_1)$ (dash-dotted line), $\text{Im}(\mathcal{K}_2)$ (dashed line), and $\text{Im}(K)$ (solid line). System parameters are given by $\Gamma_{j2} \approx \Gamma_{j3}$ $(j = 1,4) = 4.08 \times 10^7$ Hz, $\gamma_{32}^{\text{col}} \approx \gamma_{21}^{\text{col}} \approx \gamma_{31}^{\text{col}} = 5 \times 10^6$ Hz, $\gamma = 3 \times 10^6$ Hz, $\Omega_c = 220$ MHz, and $\Delta\omega_D = 0.6$ GHz. We see that $\text{Im}(\mathcal{K}_1)$ is positive but $\text{Im}(\mathcal{K}_2)$ is negative. However, their superposition, which gives $\text{Im}(K)$, is positive and displays an absorption doublet with a significant transparency window near $\omega = 0$. Because a destructive interference exists in the probe-field absorption spectrum, the phenomenon found here should be attributed to an EIT according to the criterion given in Refs. [15–17]. Such EIT can be taken as the one induced by the Doppler effect. The reason is that when the Doppler broadening is absent, the negative $\text{Im}(\mathcal{K}_2)$ term does not exist, and hence only an absorption spectrum with a positive single peak [i.e., the dash-dotted line contributed by $\text{Im}(\mathcal{K}_1)$] appears.

(ii) *Large control-field region* (i.e., $\Omega_c > \Omega_{\text{ref}}$): By extending the approach of Agarwal [14], we can decompose $\text{Im}(\mathcal{K}_j)$ $(j = 1,2)$ as

$$\text{Im}(\mathcal{K}_j) = \alpha_j\left\{\frac{1}{2}\left[\frac{W_j}{\left(\omega - \delta_j^r\right)^2 + W_j^2} + \frac{W_j}{\left(\omega + \delta_j^r\right)^2 + W_j^2}\right]\right.$$
$$\left. + \frac{g_j}{2\delta_j^r}\left[\frac{\omega - \delta_j^r}{\left(\omega - \delta_j^r\right)^2 + W_j^2} - \frac{\omega + \delta_j^r}{\left(\omega + \delta_j^r\right)^2 + W_j^2}\right]\right\},$$

(17)

where

$$W_1 = \frac{1}{2}[\gamma_{31}(1+B) + \gamma_{32}]/2, \quad \text{(18a)}$$

$$\delta_1^r = \frac{1}{2}[4|\Omega_c|^2 - [\gamma_{31}(1+B) - \gamma_{32}]^2]^{1/2}, \quad \text{(18b)}$$

$$g_1 = \frac{\gamma_{31}(1+B) - \gamma_{32}}{2} + \frac{\Gamma_3|\Omega_c|^2(1+B)}{\Gamma_3(1-B^2)\gamma_{31} + 2|\Omega_c|^2} \quad \text{(18c)}$$

and

$$W_2 = \frac{1}{2}(\gamma_{31} + \Delta\omega_D + \gamma_{32}), \quad \text{(19a)}$$

$$\delta_2^r = \frac{1}{2}[4|\Omega_c|^2 - (\gamma_{31} + \Delta\omega_D - \gamma_{32})^2], \quad \text{(19b)}$$

$$g_2 = \frac{\gamma_{31} + \Delta\omega_D - \gamma_{32}}{2} + \frac{\Gamma_3|\Omega_c|^2(\gamma_{31} + \Delta\omega_D)}{\Gamma_3(\gamma_{31}^2 - \Delta\omega_D^2) + 2\gamma_{31}|\Omega_c|^2}. \quad \text{(19c)}$$

Obviously, terms in the first square bracket on the right-hand side of Eq. (17) are two Lorentzians, which are the net contribution to probe-field absorption from two different channels corresponding to the two dressed states created by the control field Ω_c, with W_j being the width (also strength) of the two Lorentzians and δ_j^r being the real part of the spectrum poles. The following terms in the second square bracket are clearly quantum interference ones (which are called dispersive terms by Agarwal [14]). Obviously, the magnitude
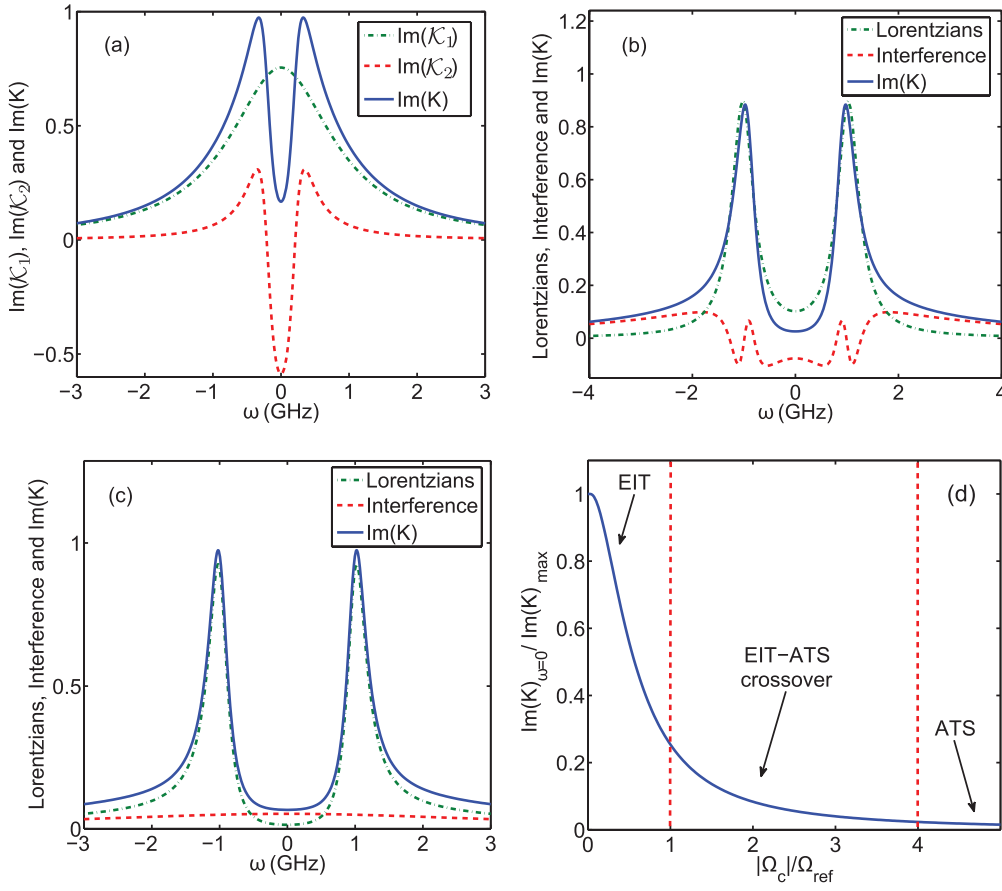
FIG. 3. (Color online) EIT-ATS crossover for hot molecules in the copropagating configuration. (a) $\text{Im}(\mathcal{K}_1)$ (dash-dotted line), $\text{Im}(\mathcal{K}_2)$ (dashed line), and $\text{Im}(\mathcal{K})$ (solid line) as functions of ω for $\Omega_c < \Omega_{\text{ref}} \equiv \Delta\omega_D/2$. (b) Absorption spectrum contributed by two Lorentzians (dash-dotted line), destructive interference (dashed line), and total absorption spectrum $\text{Im}(K)$ (solid line), in the region $\Omega_c > \Omega_{\text{ref}}$. (c) Absorption spectrum contributed by two Lorentzians (dash-dotted line), small constructive interference (dashed line), and total absorption spectrum $\text{Im}(K)$ (solid line), in the region $\Omega_c \gg \Omega_{\text{ref}}$. (a) EIT, (b) EIT-ATS crossover, and (c) ATS regions. (d) Transition from EIT to ATS for hot molecules in the copropagating configuration. Shown is $\text{Im}(K)_{\omega=0}/\text{Im}(K)_{\text{max}}$ as a function of $|\Omega_c|/\Omega_{\text{ref}}$. Three regions (EIT, EIT-ATS crossover, and ATS) are divided by the two dashed vertical lines.

of the interference is controlled by the parameter g_j. If $g_j > 0$ ($g_j < 0$), the interference is destructive (constructive).

Shown in Fig. 3(b) are results of the probe-field absorption as functions of ω for $\Omega_c > \Omega_{\text{ref}}$. The dash-dotted line (dashed line) denotes the contribution by the sum of the Lorentzian terms (interference terms) in $\text{Im}(K)$ [$=\text{Im}(\mathcal{K}_1) + \text{Im}(\mathcal{K}_2)$]. We see that the interference is destructive, and interestingly, some structures appear. The solid line gives the result of $\text{Im}(K)$. System parameters used in the plot are the same as those in Fig. 3(a) but with $\Omega_c = 1$ GHz. Clearly, a wide and deep transparency window is opened and the phenomenon found can be attributed to EIT-ATS crossover.

(iii) *Strong control-field region* (i.e., $\Omega_c \gg \Omega_{\text{ref}}$): In this region, the quantum interference strength g_j/δ_j^r in Eq. (17) is very weak and negligible. We have

$$\text{Im}(\mathcal{K}_j) \approx \frac{\alpha_j}{2}\left(\frac{W_j}{\left(\omega - \delta_j^r\right)^2 + W_j^2} + \frac{W_j}{\left(\omega + \delta_j^r\right)^2 + W_j^2}\right), \quad (20)$$

being the sum of two equal-width Lorentzians shifted from the origin by $\delta_j^r \approx \pm\Omega_c$ ($j = 1,2$).

Shown in Fig. 3(c) are results of the probe-field absorption as functions of ω for $\Omega_c \gg \Omega_{\text{ref}}$. The dash-dotted line represents the contribution by the sum of the two Lorentzian terms. For illustration, we have also plotted the contribution from the interference terms [neglected in Eq. (20)], denoted by the dashed line. We see that the interference is constructive but very small. The solid line is the curve of $\text{Im}(K)$, which has two resonances at $\omega \approx \pm\Omega_c$. Parameters used are the same as those in Figs. 3(a) and 3(b) but with $\Omega_c = 1.8$ GHz. Obviously, the phenomenon found in this situation belongs to ATS because the transparency window opened in this case is mainly due to the contribution of the two Lorentzians.

The above results show that the probe-field absorption spectrum experiences a transition from EIT to ATS as the control-field Rabi frequency Ω_c is changed from weak to strong values. Essentially, one can obtain three different regions of the probe absorption spectrum according to the value of $|\Omega_c|/\Omega_{\text{ref}}$. The first is the EIT region ($|\Omega_c|/\Omega_{\text{ref}} \leqslant 1$), where the quantum destructive interference by the Doppler effect results in the appearance of a transparency window. The second is the region of EIT-ATS crossover ($1 \leqslant |\Omega_c|/\Omega_{\text{ref}} \leqslant 4$),

where both quantum destructive interference and ATS exist together. Note that we have defined $\mathrm{Im}(K)_{\omega=0}/\mathrm{Im}(K)_{\mathrm{max}} = 0.01$ as the border between the EIT-ATS crossover and the ATS regions. The third is the ATS region ($|\Omega_c|/\Omega_{\mathrm{ref}} > 4$), where $\mathrm{Im}(K)_{\omega=0}/\mathrm{Im}(K)_{\mathrm{max}} \leqslant 0.01$ and the transparency window is contributed only by the two Lorentzians. Figure 3(d) shows a "phase diagram" that illustrates the transition from the EIT to the ATS region by plotting $\mathrm{Im}(K)_{\omega=0}/\mathrm{Im}(K)_{\mathrm{max}}$ as a function of $|\Omega_c|/\Omega_{\mathrm{ref}}$.

3. Comparison with experiment

To verify our theoretical result given above, it is necessary to make a quantitative comparison with the experimental one reported recently by Lazoudis *et al.* [9]. By using the parameters $\Gamma_{12} = \Gamma_{13} = \Gamma_{42} = \Gamma_{43} = 4.08 \times 10^7$ Hz, $\gamma = 3\mathrm{MHz}$, $\gamma_{jl}^{\mathrm{col}} \approx 5$ MHz, and $\Delta\omega_D = 1.2$ GHz, we calculate the absorption spectrum $\mathrm{Im}(K)$ for the case of the copropagating configuration, with results plotted as the dashed lines in Fig. 4. Figure 4(a) is the control field on resonance with $\Omega_c = 220$ MHz, where a sharp dip appears in the center of the absorption

spectrum and the absorption doublet is symmetric. Figure 4(b) is the control field detuned 100 MHz with $\Omega_c = 190$ MHz, where a sharp dip also occurs but the absorption doublet is asymmetric. One can see that our theoretical results (dashed lines) are very close to the experimental ones measured by Lazoudis *et al.* [9], which are represented by the solid lines. Note in passing that here we have plotted the quantity $\mathrm{Im}K$, which is proportional to the fluorescence intensity related to state $|3\rangle$ because $\sigma_{33} = 2|\Omega_p|^2\mathrm{Im}(K)/(\gamma + \Gamma_3)$. According to Eq. (13), the width of the transparency window Γ_{TW}, which is calculated to be 0.24 GHz, agrees well with the experimental one reported in Ref. [9]. We stress that the system is in the region of the weak control field (i.e., $\Omega_c \ll \Omega_{\mathrm{ref}} = \Delta\omega_D/2$), so the phenomenon observed by Lazoudis *et al.* [9] is indeed an EIT phenomenon assisted by the Doppler effect.

B. Counter-propagating configuration

In this case, one has $d_{31} = \Delta_3 - k_p v + i\gamma_{31}$, $d_{21} = \Delta_2 + k_p v + i\gamma_{21}$, and $d_{32} = \Delta_3 - \Delta_2 - 2k_p v + i\gamma_{32}$. Similarly, one can obtain the dispersion relation with the form

$$K = \frac{\omega}{c} + \mathcal{K}_1(\omega) + \mathcal{K}_2(\omega), \tag{21a}$$

$$\mathcal{K}_1 = \kappa'_{13} \frac{(\omega + i\gamma_{32})\Delta\omega_D[\Gamma_3(1 - B^2)\gamma_{31} + 2|\Omega_c|^2] - i\Delta\omega_D\Gamma_3|\Omega_c|^2(1 - B)}{\gamma\Gamma_3 B(\Delta\omega_D^2 - B^2\gamma_{31}^2)[|\Omega_c|^2 - (\omega + iB\gamma_{31} + i\gamma_{31})(\omega + i2B\gamma_{31} + i\gamma_{32})]}, \tag{21b}$$

$$\mathcal{K}_2 = \kappa'_{13} \frac{(\omega + i\gamma_{32} + i2\Delta\omega_D)[(\gamma_{31}^2 - \Delta\omega_D^2) + |\Omega_c|^2] - i|\Omega_c|^2(\gamma_{31} - \Delta\omega_D)}{[\gamma(\gamma_{31}^2 - \Delta\omega_D^2) + |\Omega_c|^2\Gamma_{13}][|\Omega_c|^2 - (\omega + i\gamma_{31} + i\Delta\omega_D)(\omega + i\gamma_{32} + i2\Delta\omega_D)]}, \tag{21c}$$

where $\mathcal{K}_1$ and $\mathcal{K}_2$ are obtained from poles $k_p v = \Delta_2 - iB\gamma_{21}$ and $k_p v = -ik_p v_T$, respectively.

We first discuss the minimum value of the absorption spectrum at $\omega = 0$, i.e., $\mathrm{Im}(K)_{\mathrm{min}}$. From Eq. (21),

we obtain

$$\mathrm{Im}(K)_{\mathrm{min}} \approx \frac{\kappa'_{13}}{\Delta\omega_D} \frac{x + z/2 + z\sqrt{x}/2 + 2\sqrt{x}/z}{(1 + \sqrt{x})(x + \sqrt{x}/z + z/2)(1 + 2\sqrt{x}/z)}, \tag{22}$$
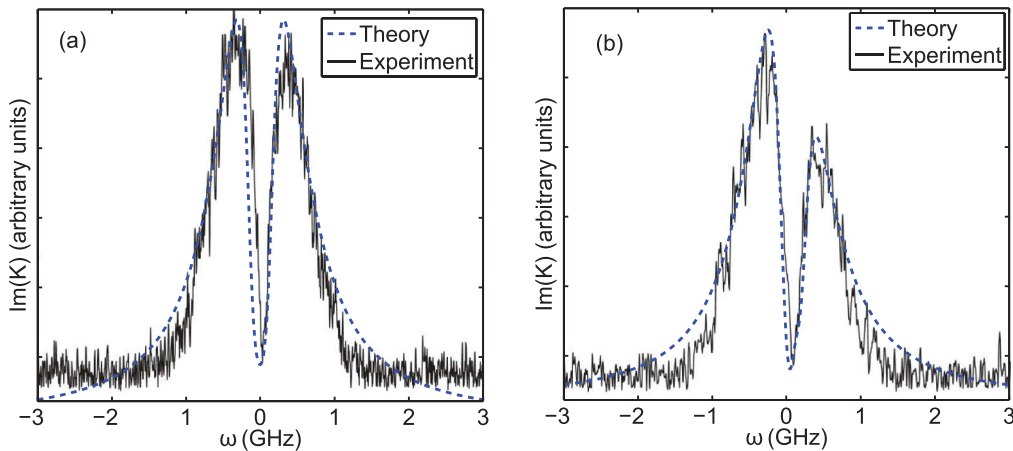

FIG. 4. (Color online) Experimental result reported by Lazoudis *et al.* [9] (solid line) and our theoretical one (dashed line) for the probe absorption spectrum in the case of the co-propagating configuration. (a) The control field is on resonance with $\Omega_c = 220$ MHz. (b) The control field is detuned 100 MHz with $\Omega_c = 190$ MHz.

where $x \equiv |\Omega_c|^2 \gamma_{31}/(2\gamma_{32}\Delta\omega_D^2)$ and $z \equiv \gamma/\Delta\omega_D$. Obviously, we have $z \ll 1$ because $\gamma \ll \Delta\omega_D$. From Eq. (22) we obtain the following conclusions:

(1) For a large $|\Omega_c|$, i.e., $|\Omega_c| \gg \sqrt{2\gamma_{32}/\gamma_{31}}\Delta\omega_D$ (and hence $x \gg 1$), $\mathrm{Im}(K)_{\min}$ is vanishing small.

(2) For a small $|\Omega_c|$, i.e., $|\Omega_c| \ll \sqrt{2\gamma_{32}/\gamma_{31}}\Delta\omega_D$ but with $|\Omega_c| \approx \sqrt{2\gamma_{32}/\gamma_{31}}\gamma$ (and hence $x \ll 1$, $\sqrt{x}/z \sim 1$), $\mathrm{Im}(K)_{\min}$ is small.

Similarly, $\mathcal{K}_j$ can be also expressed in the form of (14), with the corresponding α_j, $A_{j\pm}$, δ_{j+} and δ_{j-} given in the Appendix. We decompose $\mathrm{Im}(\mathcal{K}_j)$ according to different Ω_c values as the following.

(i) *Weak control-field region* (i.e., $\Omega_c < \Omega_{\mathrm{ref}}$): $\mathrm{Im}(\mathcal{K}_j)$ can be expressed in the form of Eq. (15), but with

$$W_{1\pm} = \tfrac{1}{2}[\gamma_{31}(1+3B)+\gamma_{32}$$
$$\pm\sqrt{[\gamma_{31}(1-B)-\gamma_{32}]^2 - 4|\Omega_c|^2}], \tag{23a}$$

$$W_{2\pm} = \tfrac{1}{2}[\gamma_{31}+\gamma_{32}+3\Delta\omega_D$$
$$\pm\sqrt{(\gamma_{31}-\gamma_{32}-\Delta\omega_D)^2 - 4|\Omega_c|^2}], \tag{23b}$$

$$\Gamma_1^w = \gamma_{32} + 2B\gamma_{31} + \Gamma_3|\Omega_c|^2(1-B)/[\Gamma_3(1-B^2)\gamma_{31}$$
$$+ 2|\Omega_c|^2], \tag{23c}$$

$$\Gamma_2^w = \gamma_{32} + 2\Delta\omega_D + \Gamma_3|\Omega_c|^2(\gamma_{31}-\Delta\omega_D)/$$
$$\times [\Gamma_3(\gamma_{31}^2 - \Delta\omega_D^2) + 2\gamma_{31}|\Omega_c|^2]. \tag{23d}$$

Shown in Fig. 5(a) are results for $\mathrm{Im}(\mathcal{K}_1)$ (dash-dotted line), $\mathrm{Im}(\mathcal{K}_2)$ (dashed line), and $\mathrm{Im}(K)$ (solid line). System parameters are given by $\Gamma_{j2} \approx \Gamma_{j3}$ ($j = 1,4$) $= 4.08 \times 10^7$ Hz, $\gamma_{32}^{\mathrm{col}} \approx \gamma_{21}^{\mathrm{col}} \approx \gamma_{31}^{\mathrm{col}} = 5 \times 10^6$ Hz, $\gamma = 3 \times 10^6$ Hz, $\Omega_c = 100$ MHz, and $\Delta\omega_D = 0.6$ GHz. Again, one has $\mathrm{Im}(\mathcal{K}_1) > 0$ and $\mathrm{Im}(\mathcal{K}_2) < 0$. Their sum gives the total absorption $\mathrm{Im}(K)$, which displays an absorption doublet with a significant transparency window near $\omega = 0$. This remarkable feature comes also from the destructive interference induced by the Doppler effect because the negative $\mathrm{Im}(\mathcal{K}_2)$ term disappears if the Doppler broadening is absent. According to the criterion given in Refs. [15–17], this phenomenon belongs to EIT. However, the counter-propagating configuration results in a mismatch of beam detunings relative to each other, and hence although a transparency window due to the Doppler effect is opened, it is relatively shallow compared with the case of the copropagating configuration.

(ii) *Large control-field region* (i.e., $\Omega_c > \Omega_{\mathrm{ref}}$): By extending the approach of Agarwal [14], we obtain $\mathrm{Im}(\mathcal{K}_j)$ ($j = 1,2$),
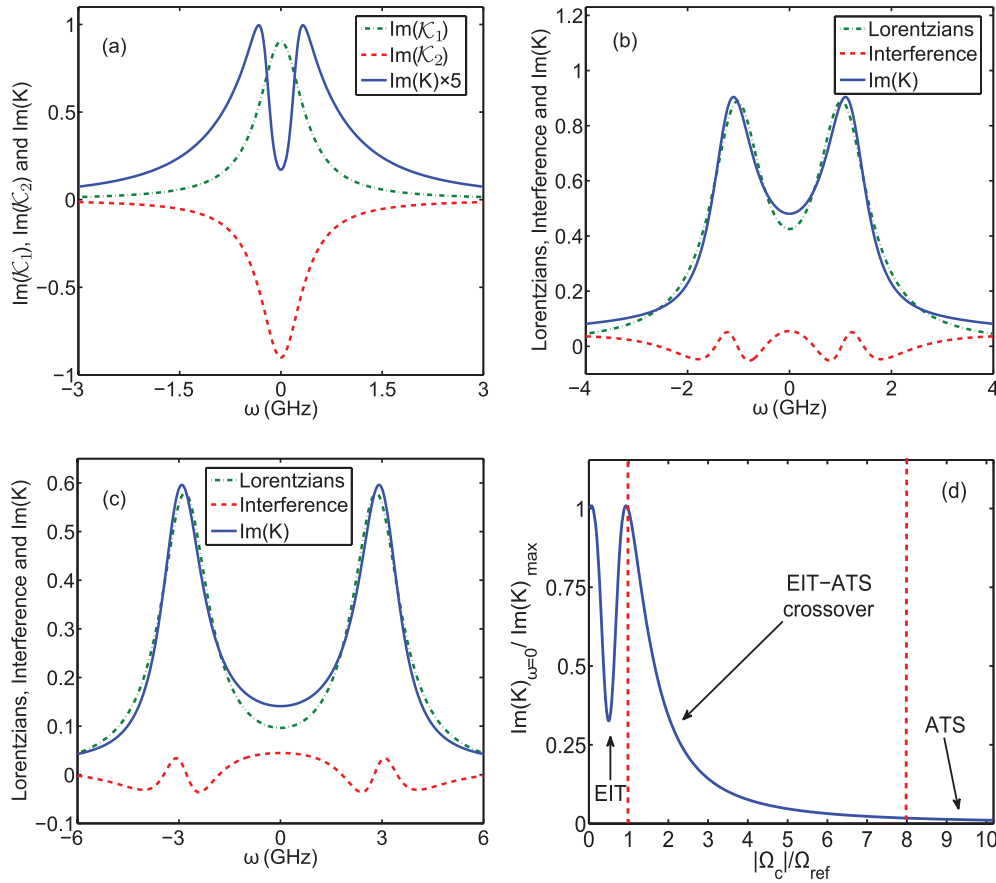

FIG. 5. (Color online) EIT-ATS crossover for hot molecules in the counter-propagating configuration. (a) $\mathrm{Im}(\mathcal{K}_1)$ (dash-dotted line), $\mathrm{Im}(\mathcal{K}_2)$ (dashed line), and $\mathrm{Im}(K)$ (solid line) as a function of ω for $\Omega_c < \Omega_{\mathrm{ref}}$. (b) Absorption spectrum contributed by two Lorentzians (dash-dotted line), destructive interference (dashed line), and $\mathrm{Im}(K)$ (solid line), in the region $\Omega_c > \Omega_{\mathrm{ref}}$. (c) Absorption spectrum contributed by two Lorentzians (dash-dotted line), destructive interference (dashed line), and $\mathrm{Im}(K)$ (solid line), in the region $\Omega_c \gg \Omega_{\mathrm{ref}}$. (a) EIT, (b) EIT-ATS crossover, and (c) ATS regions. (d) Transition from EIT to ATS for hot molecules in the counter-propagating configuration. $\mathrm{Im}(K)_{\omega=0}/\mathrm{Im}(K)_{\max}$ as a function of $|\Omega_c|/\Omega_{\mathrm{ref}}$. Three regions (EIT, EIT-ATS crossover, and ATS) are divided by the two dashed vertical lines.
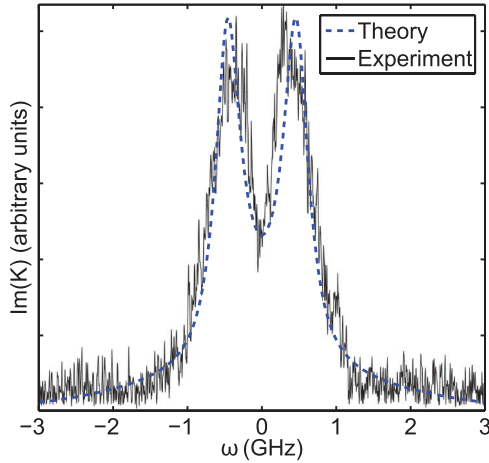
FIG. 6. (Color online) Experimental result reported by Lazoudis *et al.* [9] (solid line) and our theoretical one (dashed line) for the counter-propagating configuration. The control field is on resonance with $\Omega_c = 240$ MHz.

with the same form of Eq. (17) but with

$$W_1 = (\gamma_{31} + \gamma_{32} + 3\Delta\omega_D)/2, \tag{24a}$$

$$\delta_1^r = \sqrt{4|\Omega_c|^2 - (\gamma_{31} - \gamma_{32} - \Delta\omega_D)^2}/2, \tag{24b}$$

$$g_1 = \frac{\gamma_{31} - \gamma_{32} - \Delta\omega_D}{2} + \frac{\Gamma_3|\Omega_c|^2(\gamma_{31} - \Delta\omega_D)}{\Gamma_3(\gamma_{31}^2 - \Delta\omega_D^2) + 2\gamma_{31}|\Omega_c|^2} \tag{24c}$$

and

$$W_2 = [\gamma_{31}(1 + 3B) + \gamma_{32}]/2, \tag{25a}$$

$$\delta_2^r = \sqrt{4|\Omega_c|^2 - [\gamma_{31}(1 - B) - \gamma_{32}]^2}/2, \tag{25b}$$

$$g_2 = \frac{\gamma_{31}(1 - B) - \gamma_{32}}{2} + \frac{\Gamma_3|\Omega_c|^2(1 - B)}{\Gamma_3(1 - B^2)\gamma_{31} + 2|\Omega_c|^2}. \tag{25c}$$

(iii) *Strong control-field region* (i.e., $\Omega_c \gg \Omega_{\text{ref}}$): In this situation, the quantum interference strength g_j/δ_j^r in the decomposed probe absorption spectrum [with the same form as Eq. (17)], is very weak and the linear absorption corresponds to the sum of two Lorentzians shifted from the origin by $\delta_j^r \approx \pm\Omega_c$ ($j = 1, 2$).

Shown in Figs. 5(b) and 5(c) are results of the probe-field absorption spectra as functions of ω for $\Omega_c > \Omega_{\text{ref}}$ and $\Omega_c \gg \Omega_{\text{ref}}$, respectively. The dash-dotted line (dashed line) denotes the contribution by the sum of two Lorentzians terms (interference terms) in $\text{Im}(K)$. We see that both destructive and constructive interferences appear for different ω. The solid line gives the result of $\text{Im}(K)$. System parameters used are the same as those in Fig. 5(a), but with $\Omega_c = 1.2$ GHz and $\Omega_c = 3.0$ GHz for Figs. 5(b) and 5(c), respectively. Shown in Fig. 5(d) is the "phase diagram" that illustrates the transition from EIT to ATS for the conter-propagating configuration by plotting $\text{Im}(K)_{\omega=0}/\text{Im}(K)_{\text{max}}$ as a function of $|\Omega_c|/\Omega_{\text{ref}}$.

To test our theoretical prediction, a comparison with the experimental one for the counter-propagating configuration reported by Lazoudis *et al.* [9] is also made, as shown in Fig. 6. By using the system parameters $\Gamma_{12} = \Gamma_{13} = \Gamma_{42} = \Gamma_{43} = 4.08 \times 10^7$ Hz, $\gamma_{jl}^{\text{col}} = 5 \times 10^6$ Hz, $\gamma = 3 \times 10^6$ Hz, and $\Omega_c =$

240 MHz, the absorption spectrum $\text{Im}(K)$ is calculated based on our formulas, with the result plotted as the dashed line in the figure. We see that our theoretical result (dashed line) agrees well with the experimental one measured by Lazoudis *et al.* [9], which is denoted by the solid line.

IV. COLD MOLECULES AND COMPARISON FOR VARIOUS CASES

Our model presented in Sec. II is also valid for cold molecules. In this case, one should take $v = 0$ in the Bloch equation (2), and $f(v) = \delta(v)$ in the Maxwell equation (4). Solutions (5) and (6) are still valid but one must take $v = 0$ and the dispersion relation is changed by

$$K(\omega) = \frac{\omega}{c} + \kappa_{13}\sigma_{11}^{(0)}\frac{\omega + i\Gamma}{|\Omega_c|^2 - (\omega + i\gamma_{31})(\omega + i\gamma_{32})}, \tag{26}$$

with $\Gamma = \gamma_{32} - (\Gamma_{12}|\Omega_c|^2)/(\Gamma_{12}\gamma_{21} + 2|\Omega_c|^2)$. We have chosen $\Delta_2 = \Delta_3 = 0$ for simplicity.

The dispersion relation, (26), can also be decomposed in the form of Eq. (14), but with spectrum poles given by

$$\delta_\pm = [i(\gamma_{31} + \gamma_{32}) \pm \sqrt{4|\Omega_c|^2 - (\gamma_{31} - \gamma_{32})^2}]/2. \tag{27}$$

A spectrum decomposition similar to that done in the last section can be carried out, which is omitted here to save space. Figures 7(a)–7(c) show the results of the probe-field absorption spectrum $\text{Im}(K)$ decomposed in the weak, large, and strong control-field regions, respectively. System parameters are given by $\Gamma_{12} = \Gamma_{13} = \Gamma_{42} = \Gamma_{43} = 4.08 \times 10^7$ Hz, $\gamma_{jl}^{\text{col}} = 5 \times 10^6$ Hz, and $\sigma_{11}^{\text{eq}} = 1$ for the weak [$\Omega_c = 18$ MHz; Fig. 7(a)], large [$\Omega_c = 100$ MHz; Fig. 7(b)], and strong [$\Omega_c = 800$ MHz; Fig. 7(c)] control-field regions, respectively. We see that in Fig. 7(a) two positive single Lorentzian peaks (i.e., dashed line and dotted-dashed line) are superimposed on the absorption spectrum; their superposition is a single peak (i.e., solid line). Thus the quantum interference is constructive and hence there is no EIT in this weak control-field region. Similarly, the quantum interferences shown in Figs. 7(b) and 7(c) are also constructive. Consequently, there is no EIT or EIT-ATS crossover for cold molecules in V-type systems. Figure 7(d) shows $\text{Im}(K)_{\omega=0}/\text{Im}(K)_{\text{max}}$ for cold molecules as a function of $|\Omega_c|/\Omega_{\text{ref}}$, where $\Omega_{\text{ref}} \equiv (\gamma_{32} - \gamma_{31})/2$. Three regions (constructive interference, ATS with constructive interference, and ATS) are delineated by the two dashed vertical lines.

From these results and those given in Sec. III, we see that the quantum interference in the V-type molecular system displays very different features, which depend on the existence or nonexistence of the Doppler broadening and, also, depend on the beam propagating (copropagating or counter-propagating) configurations. For comparison, in Table I some useful physical quantities, including the EIT condition, value of $\text{Im}(K)_{\omega=0}$, group velocity v_g, and width of the transparency window Γ_{TW}, are presented for several different physical cases.

The first row in Table I is for the cold molecular system, for which no EIT exists; the second row is for the Doppler-broadened system with the copropagating configuration; and the third row is for the Doppler-broadened system with the counter-propagating configuration. Both the co- and the counter-propagating configurations allow Doppler-broadening-induced EIT, but their EIT
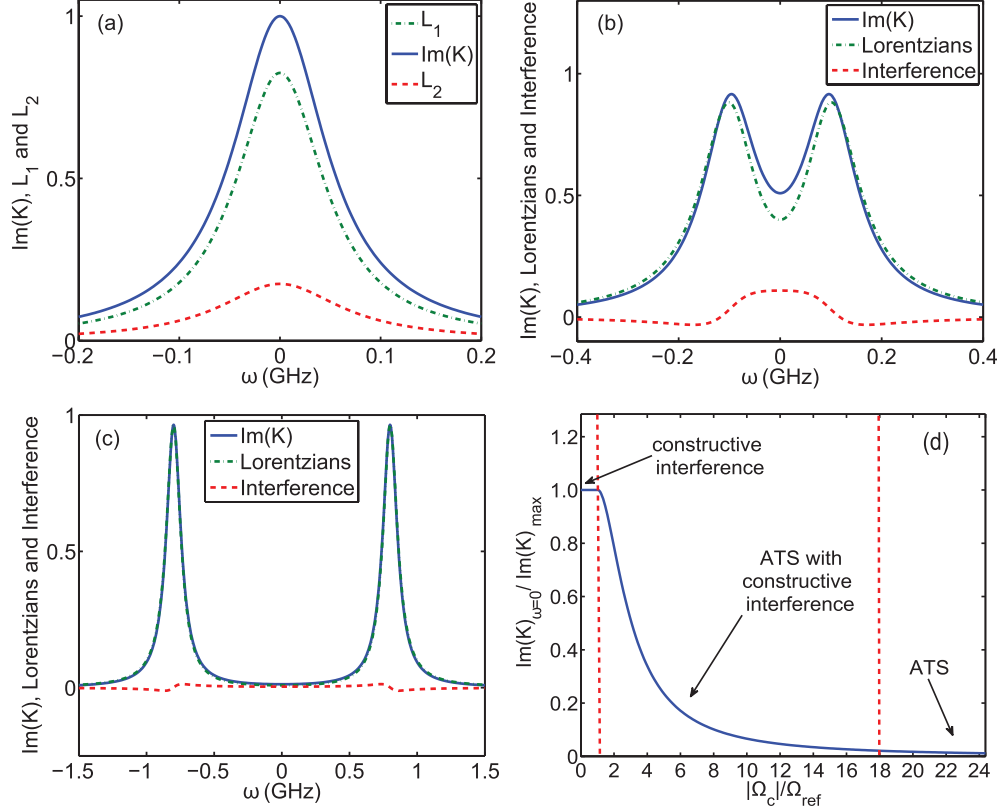
FIG. 7. (Color online) (a) A single Lorentzian peak L_1 (dash-dotted line), a single Lorentzian peak L_2 (dashed line), and Im(K) (solid line) as function of ω for $\Omega_c < \Omega_{\text{ref}}$. (b) Absorption spectrum contributed by two Lorentzians (dash-dotted line), constructive interference (dashed line), and Im(K) (solid line), in the region $\Omega_c > \Omega_{\text{ref}}$. (c) Absorption spectrum contributed by two Lorentzians (dash-dotted line), constructive interference (dashed line), and Im(K) (solid line), in the region $\Omega_c \gg \Omega_{\text{ref}}$. (d) Im($K$)$_{\omega=0}$/Im($K$)$_{\text{max}}$ for cold molecules as a function of the control field $|\Omega_c|/\Omega_{\text{ref}}$, with $\Omega_{\text{ref}} \equiv (\gamma_{32} - \gamma_{31})/2$. Three regions (constructive interference, ATS with constructive interference, and ATS) are divided by the two dashed vertical lines.

conditions are different. The value of Im(K)$_{\omega=0}$ for the copropagating configuration is much less than that of the cold molecular system and the hot molecular system with the counter-propagating configuration. However, the width of the transparency window and the group velocity are the same for both the co- and the counter-propagating configurations. These interesting features deserve to be verified by further experiments for V-type molecular systems.

V. ROLES OF SATURATION AND HOLE BURNING

Differently from the three-level Λ system [6], where only quantum interference appears, in the three-level V-type system

with inhomogeneous broadening there may be a couple of simultaneously occurring mechanisms (including saturation, hole burning, and quantum interference) contributing to the absorption of the probe field, which cannot be easily distinguished from each other. However, the density matrix formulas are able to analyze all these various contributions since they deal with both coherence and incoherence (population) effects.

The saturation effect is an incoherent phenomenon, which can be described by the difference between the average populations in states $|1\rangle$ and $|2\rangle$, i.e.,

$$\Delta_{\text{P}} = \langle \sigma_{11} \rangle - \langle \sigma_{22} \rangle, \tag{28}$$

TABLE I. Comparison of propagating properties of the probe field for various V-type molecular systems, including EIT condition, value of Im(K)$_{\omega=0}$, width of the transparency window Γ_{TW}, and group velocity v_g for three cases. Other quantities listed are defined in the text. Coprop., copropagating configuration; counter-prop., counter-propagating configuration.

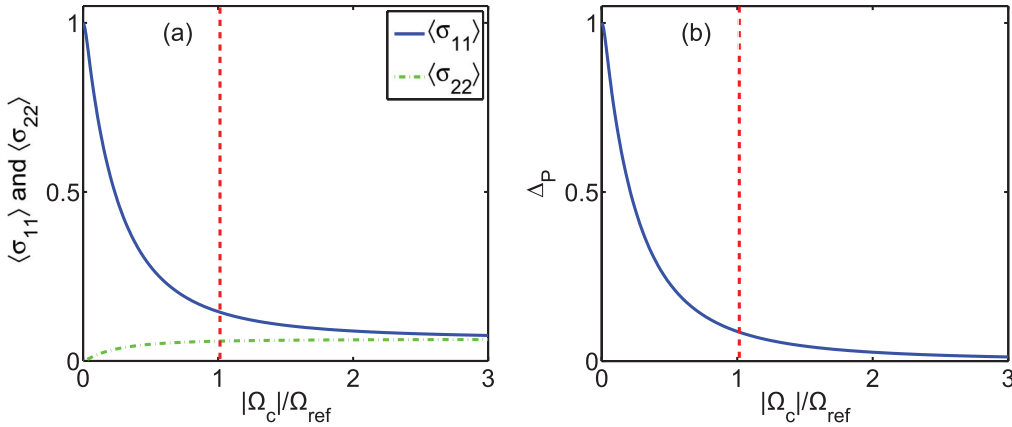| System	EIT condition	Im(K)$_{\omega=0}$	Γ_{TW}	v_g
Cold molecules	No EIT	$\frac{\kappa_{13}\gamma_{31}}{|\Omega_c|^2}$	$\frac{2|\Omega_c|^2}{\gamma_{31}}$	$\frac{|\Omega_c|^2}{\kappa_{13}}$
Hot molecules				
Coprop.	$\gamma_{31}\gamma_{32} \leqslant |\Omega_c|^2 \leqslant (\Delta\omega_D)^2/4$	$\frac{\sqrt{\pi}\kappa_{13}}{\Delta\omega_D} \frac{\gamma_{32}\Gamma_3}{\gamma_{32}\Gamma_3+|\Omega_c|^2}$	$\frac{2|\Omega_c|^2}{\Delta\omega_D}$	$\frac{|\Omega_c|^2}{\sqrt{\pi}\kappa_{13}}$
Counter-prop.	$2\gamma_{32}\gamma^2/\gamma_{31} \leqslant |\Omega_c|^2 \leqslant (\Delta\omega_D)^2/4$	$\frac{\sqrt{\pi}\kappa_{13}}{\Delta\omega_D} \frac{1}{1+|\Omega_c|/\Delta\omega_D}$	$\frac{2|\Omega_c|^2}{\Delta\omega_D}$	$\frac{|\Omega_c|^2}{\sqrt{\pi}\kappa_{13}}$

FIG. 8. (Color online) (a) Average populations $\langle\sigma_{11}\rangle$ and $\langle\sigma_{22}\rangle$ in state $|1\rangle$ (solid line) and state $|2\rangle$ (dash-dotted line) as a function of $|\Omega_c|/|\Omega_{\text{ref}}|$. (b) Average population difference Δ_{P} as a function of $|\Omega_c|/\Omega_{\text{ref}}$. The dashed vertical line in each panel is the boundary dividing the weak (left) and strong (right) control-field regions.

where $\langle\sigma_{jj}\rangle = \int_{-\infty}^{\infty} dv f(v)\sigma_{jj}$ $(j = 1,2)$, with $f(v)$ being the velocity distribution function of atoms. If Δ_{P} approaches 0, i.e. $\langle\sigma_{11}\rangle \approx \langle\sigma_{22}\rangle$, the system reaches maximum saturation. In contrary, if $\langle\sigma_{22}\rangle \ll \langle\sigma_{11}\rangle$, the saturation can be negligible. To analyze the saturation effect in our system, using the result given in Sec. II, we calculated $\langle\sigma_{11}\rangle$ and $\langle\sigma_{22}\rangle$, which are plotted in Fig. 8(a). We see that in the weak control-field region (i.e., the left side of the dashed vertical line), $\langle\sigma_{11}\rangle$ is much lager than $\langle\sigma_{22}\rangle$. Shown in Fig. 8(b) is the result of Δ_{P}. These results demonstrate that the saturation effect is significant only for a very strong control field (i.e., $|\Omega_c|/\Omega_{\text{ref}} \gg 1$). In the weak control-field region the saturation effect can be neglected.

Optical hole burning is an incoherent phenomenon where a saturating field burns a hole in the population distribution for an inhomogeneous broadened medium, which is usually called the Lamb (or Bennet) hole when reflected in the absorption spectrum of a probe field [24]. In our case, the control field is coupled to states $|1\rangle$ and $|2\rangle$, and the population in state $|1\rangle$ indeed decreases when Ω_c increases, as shown in Fig. 8(a). However, this phenomenon cannot be recognized as a hole burning. The reasons are the following. First, although for the transition $|1\rangle \leftrightarrow |3\rangle$ coupled by the probe field the control field is formally equivalent to a saturating field, this saturation field has a large detuning to state $|3\rangle$. As a result, even if a hole-burning effect exists, this effect is negligibly weak. Second, in the absorption spectrum of the probe field shown in Fig. 3, no Lamb hole appears, which can be taken as a signature of optical hole burning [25]. A simple analysis shows that the main reason for the reduction of $\langle\sigma_{11}\rangle$ comes from the effect of the transient rate γ, together with the population transfer induced by the control field.

Differently from the above two incoherent effects, which may occur in two-level systems, the EIT is a quantum interference phenomenon occurring in multilevel (at least three) systems. From the above discussion we see that in the weak control-field region neither saturation nor hole burning plays a significant role. Thus the main reason for the reduction in probe-field absorption in the weak control-field region is due to another mechanism. As shown clearly in Fig. 3(a), where the absorption spectrum of the probe field consists of a positive [i.e., dashed (red) line] and a negative [i.e., dashed-dotted

(green) line] part, the reduction in the center of the probe-field absorption spectrum is caused by destructive interference, a typical characteristic of EIT. A similar characteristic occurs also in cold three-level Λ systems as demonstrated in Ref. [17], where EIT occurs in the weak control-field region in the same way [i.e., Im(K) consists of two Lorentzians; one is positive and the other is negative]. When Ω_c increases to a large value, the saturation and hole-burning effects begin to play roles. However, the ATS effect comes into play for large Ω_c and dominates over the saturation and hole-burning effects when Ω_c becomes strong. Consequently, a crossover from EIT to ATS indeed exists in the system.

VI. SUMMARY

We have studied EIT and ATS in open V-type molecular systems. A systematic analytical approach to the probe-field absorption spectrum has been developed using the residue theorem and spectrum-decomposition method. We have found that EIT can occur and a transition from EIT to ATS exists for hot molecules. However, there is no EIT and thus no EIT-ATS crossover for cold molecules. Furthermore, we have demonstrated that for hot molecules EIT is possible even for a counter-propagating configuration. We have provided explicit formulas for EIT conditions and widths of transparency windows of the probe field when hot molecules with Doppler broadening work in copropagating and counter-propagating configurations, respectively. Our theoretical result agrees well with the recent experimental one reported by Lazoudis *et al.* [9]. Theoretical predictions presented in this work are useful to guide new experimental findings in coherent molecular systems and may have promising practical applications in coherent molecular spectroscopy, precision measurement, molecular quantum state control, and so on.

APPENDIX: EXPRESSIONS OF α, $A_{j\pm}$, AND $\delta_{j\pm}$

(i) For the copropagating configuration,

$$\alpha_1 = \kappa'_{13} \frac{\Gamma_3(1 - B^2)\gamma_{31} + 2|\Omega_c|^2}{\gamma \Gamma_3 B \left(\Delta\omega_D^2 - B^2\gamma_{31}^2\right)}, \tag{A1a}$$

$$\alpha_2 = \kappa'_{13} \frac{\Gamma_3\left(\gamma_{31}^2 - \Delta\omega_D^2\right) + 2\gamma_{31}|\Omega_c|^2}{\gamma \Gamma_3\left(\gamma_{31}^2 - \Delta\omega_D^2\right) + 2\gamma_{31}|\Omega_c|^2 \Gamma_{13}}, \tag{A1b}$$

$$A_{1\pm} = \pm \left\{ \delta_{1\pm} + i \left[\gamma_{32} - \frac{\Gamma_3|\Omega_c|^2(1 + B)}{\Gamma_3(1 - B^2)\gamma_{31} + 2|\Omega_c|^2} \right] \right\} \bigg/ (\delta_{1-} - \delta_{1+}), \tag{A1c}$$

$$A_{2\pm} = \pm \left\{ \delta_{2\pm} + i \left[\gamma_{32} - \frac{\Gamma_3|\Omega_c|^2(\gamma_{31} + \Delta\omega_D)}{\Gamma_3\left(\gamma_{31}^2 - \Delta\omega_D^2\right) + 2\gamma_{31}|\Omega_c|^2} \right] \right\} \bigg/ (\delta_{2-} - \delta_{2+}), \tag{A1d}$$

$$\delta_{1\pm} = \frac{1}{2}\{i\left[\gamma_{31}(1 + B) + \gamma_{32}\right] \pm \sqrt{4|\Omega_c|^2 - [\gamma_{31}(1 + B) - \gamma_{32}]^2}\}, \tag{A1e}$$

$$\delta_{2\pm} = \frac{1}{2}[i(\gamma_{31} + \Delta\omega_D + \gamma_{32}) \pm \sqrt{4|\Omega_c|^2 - (\gamma_{31} + \Delta\omega_D - \gamma_{32})^2}]. \tag{A1f}$$

(ii) For the counter-propagating configuration,

$$\alpha_1 = \kappa'_{13} \frac{\Delta\omega_D \Gamma_3(1 - B^2)\gamma_{31} + 2|\Omega_c|^2}{\gamma \Gamma_3 B \left(\Delta\omega_D^2 - B^2\gamma_{31}^2\right)}, \tag{A2a}$$

$$\alpha_2 = \kappa'_{13} \frac{\left(\gamma_{31}^2 - \Delta\omega_D^2\right) + |\Omega_c|^2}{\gamma \left(\gamma_{31}^2 - \Delta\omega_D^2\right) + |\Omega_c|^2 \Gamma_{13}}, \tag{A2b}$$

$$A_{1\pm} = \pm \left\{ \delta_{1\pm} + i \left[\gamma_{32} + 2B\gamma_{31} + \frac{\Gamma_3|\Omega_c|^2(1 - B)}{\Gamma_3(1 - B^2)\gamma_{31} + 2|\Omega_c|^2} \right] \right\} \bigg/ (\delta_{1-} - \delta_{1+}), \tag{A2c}$$

$$A_{2\pm} = \pm \left\{ \delta_{2\pm} + i \left\{ \gamma_{32} + 2\Delta\omega_D + \frac{\Gamma_3|\Omega_c|^2(\gamma_{31} - \Delta\omega_D)}{\Gamma_3\left(\gamma_{31}^2 - \Delta\omega_D^2\right) + 2\gamma_{31}|\Omega_c|^2} \right\} \right\} \bigg/ (\delta_{2-} - \delta_{2+}), \tag{A2d}$$

$$\delta_{1\pm} = \frac{1}{2}\{i\left[\gamma_{31}(1 + 3B) + \gamma_{32}\right] \pm \sqrt{4|\Omega_c|^2 - [\gamma_{31}(1 - B) - \gamma_{32}]^2}\}, \tag{A2e}$$

$$\delta_{2\pm} = \frac{1}{2}[i(\gamma_{31} + \gamma_{32} + 3\Delta\omega_D)/ \pm \sqrt{4|\Omega_c|^2 - (\gamma_{31} - \gamma_{32} - \Delta\omega_D)^2}]. \tag{A2f}$$

---

[1] S. R. Autler and C. R. Townes, Phys. Rev. **100**, 703 (1955).

[2] U. Fano, Phys. Rev. **124**, 1866 (1961).

[3] M. Fleischhauer, A. Imamoglu, and J. P. Marangos, Rev. Mod. Phys. **77**, 633 (2005).

[4] K. B. Khurgin and R. S. Tucker (eds.), *Slow Light: Science and Applications* (CRC, Taylor and Francis, Boca Raton, FL, 2009).

[5] J. Qi, F. C. Spano, T. Kirova, A. Lazoudis, J. Magnes, L. Li, L. M. Narducci, R. W. Field, and A. M. Lyyra, Phys. Rev. Lett. **88**, 173003 (2002).

[6] A. Lazoudis, T. Kirova, E. H. Ahmed, L. Li, J. Qi, and A. M. Lyyra, Phys. Rev. A **82**, 023812 (2010).

[7] L. Li, P. Qi, A. Lazoudis, E. Ahmed, and A. M. Lyyra, Chem. Phys. Lett. **403**, 262 (2005).

[8] A. Lazoudis, E. H. Ahmed, L. Li, T. Kirova, P. Qi, A. Hansson, J. Magnes, and A. M. Lyyra, Phys. Rev. A **78**, 043405 (2008).

[9] A. Lazoudis, T. Kirova, E. H. Ahmed, P. Qi, J. Huennekens, and A. M. Lyyra, Phys. Rev. A **83**, 063419 (2011).

[10] S. Ghosh, J. E. Sharping, D. G. Ouzounov, and A. L. Gaeta, Phys. Rev. Lett. **94**, 093902 (2005).

[11] F. Benabid and P. J. Roberts, J. Mod. Opt. **58**, 87 (2011).

[12] P. S. Light, F. Benabid, G. J. Pearce, F. Couny, and D. M. Bird, Appl. Phys. Lett. **94**, 141103 (2009).

[13] H. Li, H. Chen, M. A. Gubin, Y. V. Rostovtsev, V. A. Sautenkov, and M. O. Scully, Laser Phys. **20**, 1725 (2010).

[14] G. S. Agarwal, Phys. Rev. A **55**, 2467 (1997).

[15] P. Anisimov and O. Kocharovskaya, J. Mod. Opt. **55**, 3159 (2008).

[16] T. Y. Abi-Salloum, Phys. Rev. A **81**, 053836 (2010).

[17] P. M. Anisimov, J. P. Dowling, and B. C. Sanders, Phys. Rev. Lett. **107**, 163604 (2011).

[18] L. Giner *et al.*, Phys. Rev. A **87**, 013823 (2013).

[19] A. Javan, O. Kocharovskaya, H. Lee, and M. O. Scully, Phys. Rev. A **66**, 013805 (2002).

[20] H. Lee, V. Rostovtsev, C. J. Bednar, and A. Javan, Appl. Phys. B **76**, 33 (2003).

[21] The frequency and wave vector of the probe field are given by $\omega_p + \omega$ and $k_p + K(\omega)$, respectively. Thus $\omega = 0$ corresponds to the center frequency of the probe field.

[22] F. W. Byron and R. W. Fuller, *Mathematics in Classical and Quantum Physics*, Vol. 2 (Addison-Wesley, New York, 1969), Chap. 6.

[23] H. Lee, Y. Rostovtsev, and M. O. Scully, Phys. Rev. A **62**, 063804 (2000).

[24] X.-G. Wei, J.-H. Wu, H.-H. Wang, A. Li, Z.-H. Kang, Y. Jiang, and J.-Y. Gao, Phys. Rev. A **74**, 063820 (2006).

[25] P. Dong and J.-Y. Gao, Phys. Lett. A **265**, 52 (2000).